



This is the accepted manuscript made available via CHORUS. The article has been published as:

Electronic structure and anharmonic phonon mode in $\text{Ba}_{1-x}\text{Ge}_x$ with two-dimensional Ba-Ge networks studied by photoemission spectroscopy

Tatsuhiko Ishida, Daiki Ootsuki, Shigeyuki Ishida, Miho Kitamura, Koji Horiba, Yasumasa Takagi, Akira Yasui, Eiji Ikenaga, Kenji Kawashima, Yousuke Yanagi, Akira Iyo, Hiroshi Eisaki, and Teppei Yoshida

Phys. Rev. B **107**, 045116 — Published 12 January 2023

DOI: [10.1103/PhysRevB.107.045116](https://doi.org/10.1103/PhysRevB.107.045116)

Electronic structure and anharmonic phonon mode in BaIr_2Ge_7 with two-dimensional Ba-Ge networks studied by photoemission spectroscopy

Tatsuhiko Ishida¹, Daiki Ootsuki^{1,*}, Shigeyuki Ishida², Miho Kitamura³,
Koji Horiba^{3,†}, Yasumasa Takagi⁴, Akira Yasui⁴, Eiji Ikenaga⁴, Kenji Kawashima^{2,5},
Yousuke Yanagi^{2,5}, Akira Iyo², Hiroshi Eisaki², and Teppei Yoshida¹

¹*Graduate School of Human and Environmental Studies,
Kyoto University, Sakyo-ku, Kyoto 606-8501, Japan.*

²*National Institute of Advanced Industrial Science
and Technology (AIST), Tsukuba 305-8568, Japan.*

³*Institute of Materials Structure Science,
High Energy Accelerator Research Organization (KEK), Tsukuba, Ibaraki 305-0801, Japan.*

⁴*SPring-8/JASRI, 1-1-1 Koto, Sayo-cho, Hyogo 679-5198, Japan. and*

⁵*IMRA Material R&D Co., Ltd, Kariya, Aichi 448-0032, Japan.*

(Dated: November 28, 2022)

Abstract

We report the electronic structure of BaIr_2Ge_7 with two types of cage structure by means of angle-resolved photoemission spectroscopy (ARPES) and hard x-ray photoemission spectroscopy (HAXPES). ARPES spectra reveal the three-dimensional and multiband Fermi surfaces (FSs) originating from the hybridized Ir $5d$ and Ge $4p$ orbitals. The observed FSs show the C_2 symmetry reflecting the orthorhombic $Ammm$ crystal structure of BaIr_2Ge_7 . The temperature dependence of the ARPES spectra exhibits the thermal spectral broadening and the width of the spectral peak shows a concave-downward behavior with temperature. Considering the effect of anharmonic phonon modes, we have reproduced the temperature dependence of the electrical resistivity as well as the thermal spectral broadening. The resultant renormalized phonon frequencies $\omega_{r0}^{(1)} = 146.9$ K and $\omega_{r0}^{(2)} = 70.6$ K are comparable to the Einstein temperatures estimated from the previous specific heat measurement. Our results suggest the existence of the weak anharmonic phonon modes in BaIr_2Ge_7 .

PACS numbers: 73.20.At, 73.22.Gk, 71.30.+h

* ootsuki.daiki.4z@kyoto-u.ac.jp

† Present affiliation: Institute for Advanced Synchrotron Light Source, National Institutes for Quantum and Radiological Science and Technology, 6-6-11 Aoba, Sendai, Miyagi, 980-8579, Japan.

I. INTRODUCTION

Electron-phonon coupling is one of the most fundamental interaction and has been discussed as the key for the enhancement of the superconducting temperature (T_c) in wide variety of materials such as A-15 compounds, high- T_c cuprate, iron pnictide/chalcogenide, and hydrogen sulfide[1–5]. Anharmonic lattice vibrations, so called rattling phonons, couple to the conduction electrons and are considered as one of the source of the high thermoelectric property or the unusual high- T_c superconductivity. The anharmonic phonon originates from the guest atoms encapsulated in the polyhedral cages and has been intensively discussed in the filled skutterudites LnT_4X_{12} (Ln = lanthanoid, T = transition metal, X = pnictogen)[6], Ge/Si clathrates $A_8(\text{Ge,Si})_{46}$ [7], and β -pyrochlore oxides AOs_2O_6 (A = alkaline atom)[8].

Ba-Ir/Rh-Ge ternary compounds such as BaIr_2Ge_7 , $\text{Ba}_3\text{Ir}_4\text{Ge}_{16}$, and $\text{Ba}_3\text{Rh}_4\text{Ge}_{16}$ exhibit superconductivity with $T_c = 2.5$, 5.2 , and 6.5 K, respectively[9–13]. Quite recently, Pei *et al.* have discovered the pressure-induced reemergence of superconductivity with a maximum T_c of 4.4 K for BaIr_2Ge_7 and of 4.0 K for $\text{Ba}_3\text{Ir}_4\text{Ge}_{16}$ around 40 GPa, respectively[14]. These compounds are formed by stacking of the Ir/Rh-Ge polyhedral cages encapsulated Ba atom. The crystal structure of BaIr_2Ge_7 has a orthorhombic space group of $Ammm$ with C_2 symmetry[13] as shown in Fig. 1. The electrical resistivity ρ of BaIr_2Ge_7 decreases with decreasing temperature and reveals the concave-downward behavior[10, 13]. The temperature dependence of ρ is well reproduced by the phonon-assisted Bloch-Grüneisen (BG) formula using the Debye temperature $\Theta_D = 174$ K[13] or 240 K[10]. The normal-state specific heat data for BaIr_2Ge_7 and $\text{Ba}_3\text{Ir}_4\text{Ge}_{16}$ exhibits a broad peak around ~ 20 K, suggesting the presence of the Einstein phonon mode related to the rattling of Ba atom[10]. Furthermore, Guo *et al.* reproduced the normal-state specific heat data using the sum of the Debye mode and the two Einstein modes originating from two cages. The Debye temperature and the Einstein temperature were estimated to be $\Theta_D = 303$ K, $\Theta_{E1} = 118$ K, and $\Theta_{E2} = 60$ K for BaIr_2Ge_7 [10]. Noted that there is the difference between the Debye temperatures obtained from the electrical resistivity and the specific heat capacity. Although the existence of the Einstein modes has been proposed, Ishida *et al.* suggested that the atomic displacement parameters (ADP) for both compounds are relatively small and deviate from the other rattling materials such as β -pyrochlores, clathrates, and skutterudites due to the smaller size of cages[13]. This suggests the absence of the rattling behavior in BaIr_2Ge_7 and $\text{Ba}_3\text{Ir}_4\text{Ge}_{16}$ [13].

Therefore, the presence of the rattling phonon and the relationship between the rattling and the superconductivity are controversial.

In this context, we have performed angle-resolved photoemission spectroscopy (ARPES) and hard x-ray photoemission spectroscopy (HAXPES) for BaIr_2Ge_7 in order to clarify the electronic structure and the effect of the rattling nature. The Fermi surfaces (FSs) were observed and exhibit the two fold symmetry reflecting the C_2 symmetry of the $Ammm$ crystal structure. From the HAXPES spectra, the valence band near E_F consists of the strongly hybridized Ir $5d$ and Ge $4p$ orbitals. The ARPES spectra reveal the thermal spectral broadening and the full width of half maximum (FWHM) of the spectral peak shows a $T^{1.5}$ ($T^{0.46}$) behavior for the low (high) temperature region. Assuming the existence of the anharmonic phonon modes, we discuss the relationship between the temperature dependence of the thermal broadening of the ARPES spectrum, the electrical resistivity, and the anharmonic behavior of the specific heat capacity.

II. EXPERIMENTAL SETUPS

Single crystal BaIr_2Ge_7 was prepared by the self-flux method and the arc-melting method as reported in Ref. [13]. Angle-resolved photoemission spectroscopy (ARPES) measurements were performed at BL-28A at Photon Factory (PF) with Scienta SES2002 and DA30 analyzers[16]. The total energy resolution was 30 - 40 meV for circularly polarized light $h\nu = 40 - 120$ eV. The measurement chamber was maintained in ultra-high vacuum of higher than 3.0×10^{-10} Torr. For the temperature dependent measurement, the temperature was tuned from $T = 10$ to 190 K and the incident photon energy was set to $h\nu = 55$ eV. HAXPES measurements were carried out at BL47XU of SPring-8 with a Scienta R4000 electron analyzer. The incident photon energy was set to $h\nu = 7940$ eV with the linear polarized light. The total energy resolution was 280 meV for $h\nu = 7940$ eV. The HAXPES data were collected at $T = 150$ K. The base pressure of the chamber was 1.0×10^{-10} Torr. To obtain clean surfaces for the photoemission measurements, the samples were cleaved *in situ*. The binding energy was calibrated by using the Fermi edge of the gold reference. The electronic structure was calculated using the code WIEN2k[17] based on the full-potential linearized augmented plane-wave method. The calculated results were obtained in the generalized

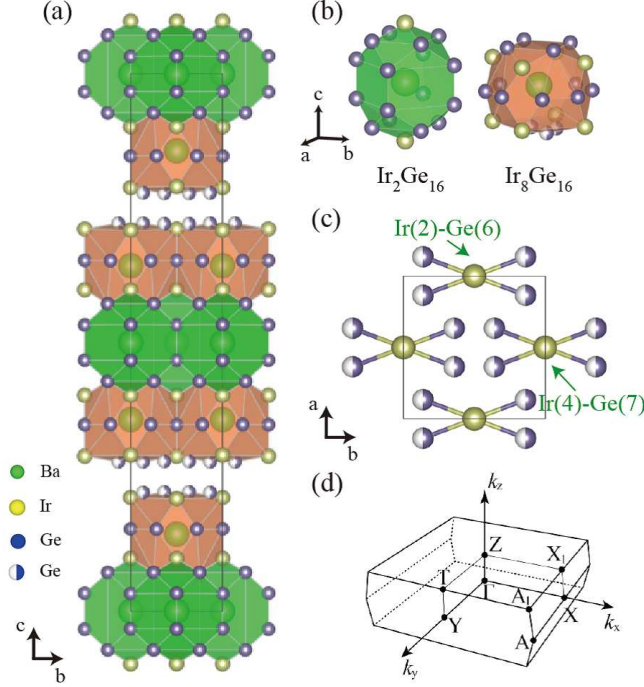


FIG. 1. (color online) (a) Crystal structure of BaIr₂Ge₇ with a space group $Ammm$ visualized by VESTA[15]. (b) Ba-centered Ir₂Ge₁₆ and Ir₈Ge₁₆ cages. The green, yellow, and blue circles indicate Ba, Ir, and Ge atoms, respectively. Here, the half-filled circle is 0.5 occupancy. The green (orange) shaded polyhedrons indicate the Ir₂Ge₁₆ (Ir₈Ge₁₆) cages which encapsulated the Ba atom. (b) Crystal structure of Ir(4)-Ge(7) plane. (c) Brillouin zone of BaIr₂Ge₇.

gradient approximation for electron correlations, where we used the exchange-correlation potential[18]. The spin-orbit interaction is taken into account and the van der Waals correction is not considered. We used the crystal structure at room temperature as reported in Ref. [13]. Because the occupancy rate of the Ge(6) and Ge(7) atoms is 0.5, the electronic structure was calculated with the half the number of Ge(6) and Ge(7) atoms, taking into account the inter atomic distance. We set the muffin-tin radii R_{MT} of 2.50 (Ba), 2.46 (Ir), and 2.18 (Ge) Bohr and the plane-wave cutoff of $K_{\text{max}} = 7.0/R_{\text{MT}}$. The calculation was carried out without the consideration of the structural relaxation.

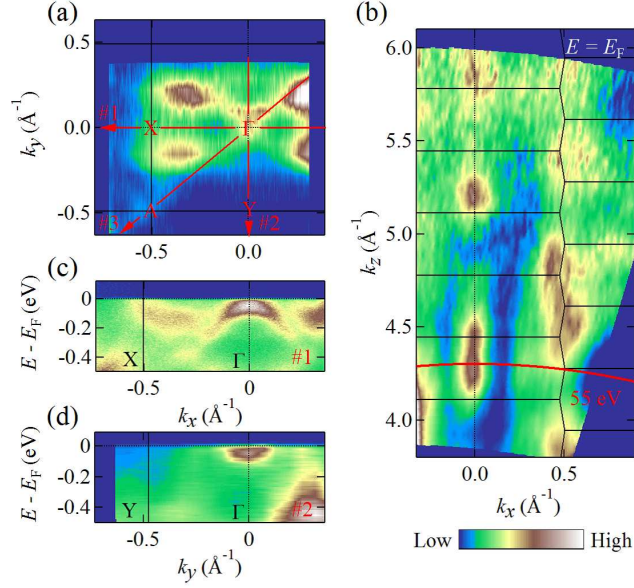


FIG. 2. (color online) ARPES intensity plots of the constant energy contours at Fermi level (E_F) of (a) $k_x - k_y$ and (b) $k_x - k_z$ planes integrated within ± 30 meV relative to E_F . Band dispersions corresponding to the cuts (c) #1 and (d) #2 in (a). The ARPES data were taken at $T = 20$ K and $h\nu = 55$ eV.

III. RESULTS AND DISCUSSION

A. Valence-band electronic structure

Figure 2(a) shows the FSs for the Γ XAY plane of Fig. 1(d) taken at $T = 20$ K and $h\nu = 55$ eV with circularly polarized light. The crossed-rectangular shaped Fermi surfaces (FSs) were observed in Fig. 2(a) and those are highly anisotropic, corresponding to the C_2 symmetry derived from the Ir(2)-Ge(6) and Ir(4)-Ge(7) planes (Fig. 1(c)). The ARPES intensity along the Γ -X direction (cut #1) and the Γ -Y direction (cut #2) were shown in Figs. 2(c) and (d), respectively. The hole band at Γ point was clearly observed in the Γ -X direction and the electron-like band can be seen in the Γ -Y direction. These results correspond to the anisotropic electronic structure of BaIr_2Ge_7 and indicate the saddle-point structure around the Γ point. Further, the several band dispersions were identified from Γ to X point (Fig. 2(c)), suggesting the multi-band nature of BaIr_2Ge_7 . Figure 2(b) shows the ARPES intensity as a function of the incident photon energy along the Γ -X direction taken at E_F . The ARPES intensity strongly depends on the incident photon energy and exhibits

the periodic modulation, suggesting the three-dimensional bulk electronic structure.

B. Core-level electronic structure

Figures 3(a),(b), and (c) show the Ba $4d$, Ir $4f$, and Ge $3p$ core-level spectra. The Ba $4d_{5/2}$ and $4d_{3/2}$ core-levels are located at 88.7 eV and 91.3 eV, respectively. The spectral shape of the Ba $4d$ core-levels of BaIr_2Ge_7 is composed of the single components, which is different from the results for the other rattling materials having the Ba guest atom[19, 20]. The single component of the Ba $4d$ core-levels implies that there is no appreciable difference of the Ba valence state between $\text{Ir}_2\text{Ge}_{16}$ and $\text{Ir}_8\text{Ge}_{16}$ cages. The binding energy of Ba $4d_{5/2}$ core-level is close to that of BaO (88.8 eV), indicating that the valence state of Ba is divalent (Ba^{2+}). Actually, the spectral shape of the Ba $4d$ core-levels is symmetric, which suggests the absence of the screening Ba $6s$ electrons at E_F . In Fig. 3(b), the Ir $4f_{7/2}$ and Ir $4f_{5/2}$ core-levels are located at 60.3 eV and 63.3 eV, respectively. The binding energy of the Ir $4f_{7/2}$ core-level for BaIr_2Ge_7 is located lower than that for IrO_2 (61.9 eV) and even that for pure Ir (60.8 eV). The lower binding energy of BaIr_2Ge_7 suggests that the Ir $5d$ orbital is strongly hybridized with the Ge $4p$ orbital and a signature of covalent bonding character. The Ge $3p_{3/2}$ and $3p_{1/2}$ core-levels are located at 121.3 eV and 125.6 eV as shown in Fig. 3(c). On the contrary to the Ba $3d$ core-levels, the Ir $4f$ and Ge $3p$ core-level line shapes are asymmetric, indicating the screening effect of the conduction electrons: the density of states (DOS) near E_F consists of the Ir $5d$ - Ge $4p$ covalent bonding state. Figure 3(d) shows the valence band spectra taken at $h\nu = 7940$ eV. The valence band spectra show the structures at ~ 0.68 , ~ 2.1 , ~ 2.9 , and ~ 4.5 eV. The observed structures can be seen in the calculated DOS and are basically consistent with the calculated DOS. The calculated DOS exhibits the strong hybridization between the Ir $5d$ and Ge $4p$ orbitals. The hybridized band of the Ir $5d$ and Ge $4p$ orbitals forms the DOS close to E_F and dominates the electronic conductivity of BaIr_2Ge_7 .

C. Temperature dependence of quasiparticle (QP) lifetime

The observed FSs and the band dispersions near E_F originate from the Ir $5d$ and Ge $4p$ orbitals in the cage structures. The expected anharmonic rattling phonon of the guest Ba

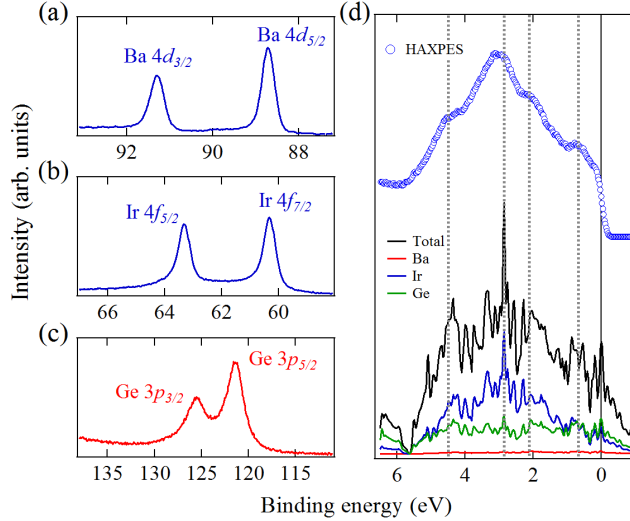


FIG. 3. (color online) HAXPES spectra of BaIr_2Ge_7 for (a) Ba $4d$, (b) Ir $4f$, and (c) Ge $3p$ core-levels. (d) Valence band spectrum compared with the calculated total and partial density of states. The data were collected at $T = 150$ K for $h\nu = 7940$ eV.

atom would couple to the electrons and be observed through the electronic structure of the cage structures. Figures 4(a) and (b) show the band dispersion and its second derivative plot along the Γ -A direction of cut #3 in Fig. 2(a) taken at $T = 10$ K for $h\nu = 55$ eV. The several bands were identified in Figs. 4(a) and (b). Figure 4(c) shows the EDCs as function of temperature from $T = 10$ to 190 K taken at Γ point (normal emission spectra). The distinct structures including the saddle point structure close to E_F and the broad hump around -0.7 eV at $T = 10$ K become broad with increasing temperature. The spectral broadening is more prominent from $T = 10$ to 75 K, whereas the spectral shape does not change significantly above $T = 75$ K. These thermal broadening behaviors suggest the decrease of the lifetime due to the phonon scattering.

In order to quantify the broadening behavior of the EDCs as a function of temperature, we have fitted the symmetrized spectra by using the Voigt functions and the Shirley background. The fitted result at $T = 10$ K as an example is shown in Fig. 4(d) and well reproduces the spectra. The peak positions of each peak were determined by the band bottom or top of the second derivative plot (indicated by red arrows in Fig. 4(b)), and the intensity rate from E_F to -0.5 eV was fixed at each temperature. Figure 4(e) shows the temperature dependence of the full width half maximum ΔE (FWHM) taken from the peak located at $E - E_F = -11$ meV. The temperature dependence of ΔE reveals the increase from $T = 10$ to 75 K and

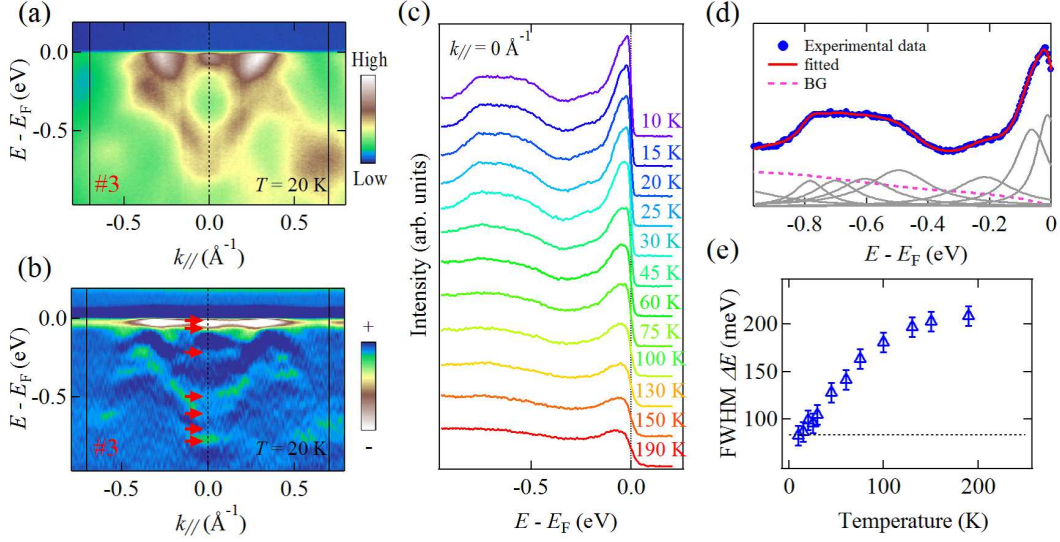


FIG. 4. (color online) (a) Band dispersion and (b) its second derivative plot along Γ -A direction (cut #3 in Fig. 2 (a)) at $T = 10$ K. (c) Temperature dependence of the energy distribution curve (EDC) taken at Γ point from $T = 10$ to 190 K. (d) Symmetrized EDC at $T = 10$ K fitted by Voigt functions. The red solid line represents the fitted curves. The gray solid lines represent the peaks of the decomposed fitting result. The peak positions correspond to the band bottom/top of (a) and are indicated by the red arrows in (b). The pink dashed line indicates the integrated background. (e) Photoemission linewidth FWHM ΔE as a function of temperature. ΔE is estimated from the peak located at $E - E_F = -11$ meV.

the gentle rise above $T = 75$ K. In general, the photoemission linewidth ΔE is proportional to the inverse of the quasiparticle lifetime \hbar/τ ($\Delta E \propto \tau^{-1}$). Here, it should be emphasized that ΔE is not equal to τ^{-1} ($\Delta E \neq \tau^{-1}$) because the ΔE includes the contribution from the width of the degenerated multiband structure. Although \hbar/τ is related to the impurity scattering, the electron-electron scattering, and the electron-phonon scattering, the main contribution of the thermal spectral broadening is due to the electron-phonon scattering. The inverse lifetime is given by

$$\tau(\epsilon, T)^{-1} = 2\pi \int_0^{\omega_{\max}} \alpha^2 F(\Omega') [1 - f(\epsilon - \Omega') + 2n(\Omega') + f(\epsilon + \Omega')] d\Omega'$$

, where $\alpha^2 F(\Omega)$ is the Eliashberg coupling function, $n(\Omega)$ and $f(\Omega)$ are the Bose-Einstein and Fermi-Dirac distribution functions, respectively[21–24]. Furthermore, the Eliashberg

function can be expressed as $\alpha^2 F(\Omega) = \lambda(\Omega/\Theta_D)$ for the Debye model and $\alpha^2 F(\Omega) = \lambda\Theta_E\delta(\Omega - \Theta_E)/2$ for the Einstein model. Following the Debye model or the simple Einstein model, τ^{-1} increases with increasing temperature and exhibits the concave upward behavior[25], which is in contrast to the concave-downward behavior of the electrical resistivity as well as that of the spectral broadening with temperature as shown in Fig. 4(e)[10, 13].

The concave-downward behavior in ρ for BaIr₂Ge₇ was well described by using the parallel resistor model of the BG term ρ_{BG} and the Ioffe-Regel (IR) saturation resistivity ρ_{max} [10, 13, 26]. However, the temperature dependence of the specific heat was reproduced by the Debye model and the Einstein model[10]. The evaluated Debye temperature differs between the estimation from the resistivity ($\Theta_D = 171$ K) and the specific heat ($\Theta_D = 303$ K)[10]. The lower Debye temperature estimated from ρ is mainly due to ρ_{max} . In the previous study[13], the ρ_{max} is estimated to be 351 $\mu\Omega\text{cm}$. The IR criterion $k_F l$ is given by $k_F l = 2\pi\hbar d/e^2\rho$, where k_F is the Fermi wave number, l is the mean free path, and d is the lattice constant. The value of $k_F l$ is evaluated to be 4.71 (27.69) from ρ_{max} for the $a(c)$ axis direction and might be large, since the carrier would be localized when $k_F l \ll 1$.

D. Anharmonic phonon

In the present study, we point out the other possible scenario causing the concave-downward behavior of ρ and ΔE . Figures 5(a) and (b) show the logarithmic plot of $\rho - \rho_0$ and $\Delta E - \Delta E_0$ as a function of temperature. The ρ_0 is the residual resistivity and the ΔE_0 is the value of ΔE at $T = 10$ K. The temperature dependence of $\rho - \rho_0$ ($\Delta E - \Delta E_0$) follows the $T^{2.28}$ ($T^{1.5}$) behavior at low temperature and the $T^{0.75}$ ($T^{0.46}$) behavior at high temperature with the inflection point around $T = 76$ K. Dahm and Ueda have proposed the T^2 dependence at low temperature and the $T^{0.5}$ at high temperature in ρ by assuming anharmonic phonon modes[27]. Following this model, the concave-downward behavior suggests the existence of anharmonic phonon modes. Hence, we have analyzed the temperature dependence of ρ and ΔE , considering the contribution of the anharmonic phonon on the basis of the Dahm and Ueda theory[27]. The phonon self-energy $\Pi(\omega)$ indicates the interaction of the phonon with the conduction electrons. The resultant renormalized phonon frequency is described as $\omega_r^2 = \omega_0^2 + 2\omega_0\text{Re}\Pi(\omega)$, where ω_0 is the effective phonon frequency.

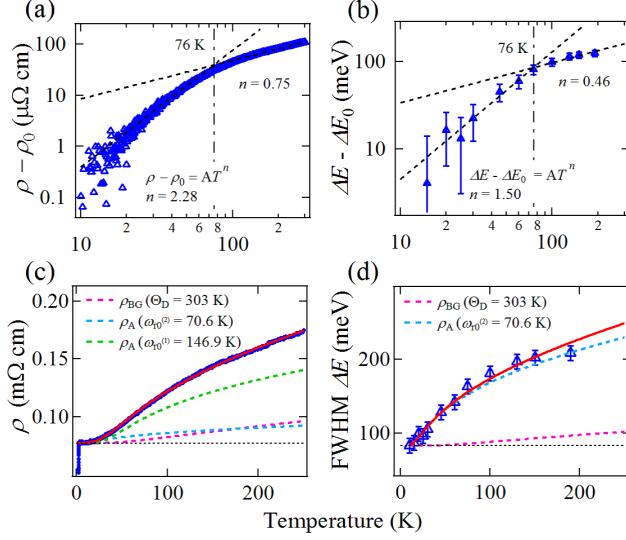


FIG. 5. (Color online) Temperature dependence of (a) electrical resistivity ρ [13] and (b) the relative variation of ΔE of Fig. 4(e) plotted on a logarithmic scale. The residual resistivity ρ_0 and the value ΔE at $T = 10$ K (ΔE_0) have been subtracted. The dashed lines indicate the $T^{2.28}$ or $T^{1.5}$ ($T^{0.753}$ or $T^{0.46}$) dependence at low (high) temperature. (c) ρ and (d) ΔE as a function of temperature and these fitted results assuming the contributions for the two anharmonic phonons with $\omega_{r0}^{(2)} = 70.6$ K and $\omega_{r0}^{(1)} = 146.9$ K and the Debye phonon with $\Theta_D = 303$ K, respectively. The dashed lines represent the each contribution from the anharmonic phonon modes (light blue and green) and Debye phonon (pink).

The temperature dependence of ω_0 follows the nonlinear equation[27]:

$$\left(\frac{\omega_0}{\omega_{00}}\right)^2 = 1 + \beta \left(\frac{\omega_{00}}{\omega_0}\right) \left(\frac{1}{e^{\hbar\omega_0/k_B T} + 1} + \frac{1}{2} - \frac{\omega_0}{2\omega_{00}}\right),$$

where β is the magnitude of the anharmonicity and $\omega_{00} = \omega_0(T = 0$ K) is the potential barrier of the double well. The phonon spectral function is expressed as

$$A(\Omega) = \frac{1}{\pi} \frac{4\omega_0\Gamma_0\Omega}{(\Omega^2 - \omega_r^2)^2 + 4\Gamma_0^2\Omega^2},$$

where Γ_0 is the temperature independent phonon damping rate[27]. The inverse of the QP lifetime τ^{-1} from the contribution of the anharmonic phonon is written as

$$\tau_A(\epsilon)^{-1} = \pi g^2 N(0) \int_0^\infty A(\Omega') [2n(\Omega') + f(\Omega' + \epsilon) + f(\Omega' - \epsilon)] d\Omega'$$

following the previous work[27, 28]. Here, g is the electron-phonon coupling constant and $N(0)$ is the DOS at E_F . The temperature dependence of $\tau_A(T)$ is described as $\tau_A(T) = \int_{-\infty}^{\infty} d\epsilon \tau_A(\epsilon) \frac{df}{d\epsilon}$ and the resistivity $\rho(T)$ is generally expressed as

$$\rho(T) = \frac{4\pi}{\omega_p^2} \tau^{-1}(T) = -\frac{4\pi}{\omega_p^2} \left[\int_{-\infty}^{\infty} d\epsilon \tau(\epsilon) \frac{df}{d\epsilon} \right]^{-1},$$

where ω_p is the plasma frequency[28]. Since the anharmonic phonon as well as the BG term[29, 30] contribute to the electrical resistivity of BaIr₂Ge₇: $\rho(T) = \rho_{BG}(T) + \rho_A(T)$, we have fitted the temperature dependence of ρ by using this model including the two anharmonic phonon modes. As shown in Fig. 5(c), the $\rho(T)$ was well fitted with the parameters : $\rho_0 = 101 \mu\Omega\text{cm}$, $\Theta_D = 303$ K, $\omega_{r0}^{(2)} = 70.6$ K and $\omega_{r0}^{(1)} = 146.9$ K, $\beta = 2.0$, $\Gamma_0 = 2$ K, and $\omega_0 \text{Re}\Pi(\omega) = -(11 \text{ K})^2$, where ω_{r0} represents the renormalized phonon frequency ω_r at $T = 0$ K. Moreover, we have also fitted the temperature dependence of $\Delta E(T)$ ($\propto \tau^{-1}(T)$) in the same manner of $\rho(T)$: $\tau(T)^{-1} = \tau_0^{-1} + \tau_A(T)^{-1} + \tau_{BG}(T)^{-1}$. Here, we set the single anharmonic phonon mode $\omega_{r0}^{(2)} = 70.6$ K for the best fit (red solid line of Fig. 5(d)) and the other parameters were the same as the fitting of $\rho(T)$. Although τ^{-1} obtained from ARPES is not identical to that measured from the transport measurement and the comparison with them must be done carefully[31], our data suggest a proportional relationship of τ^{-1} between the ARPES data and the electrical resistivity.

The renormalized phonon frequencies $\omega_{r0}^{(2)}$ and $\omega_{r0}^{(1)}$ agree to the Einstein temperatures $\Theta_{E1} = 118$ K and $\Theta_{E2} = 60$ K obtained from the normal-state specific heat data[10]. The estimated phonon frequencies $\omega_{r0}^{(2)}$ and $\omega_{r0}^{(1)}$ would be derived from the different size of the Ir₂Ge₁₆ and Ir₈Ge₁₆ cages because the reduction of the phonon frequencies is induced by the expansion of the cage. Actually, the model including the single anharmonic phonon mode well reproduces the spectral broadening. We speculated that the structure from which the lifetime is estimated derives from the Ir $5d$ and Ge $4p$ hybridized orbitals of the Ir₈Ge₁₆ cage and the anharmonic mode couples to the electrons of this cage.

The anharmonicity factor β dominates the strength of the temperature dependence of ρ and the NMR relaxation rate $1/T_1T$ as well as the thermal spectral broadening[27]. The magnitude of anharmonicity estimated to be $\beta = 2.0$ for BaIr₂Ge₇ is comparable to the filled skutterudite LaOs₄Sb₁₂ with $\beta = 2.0$ [32] and is relatively small compared with the other rattling materials such as the β -pyrochlore KOs₂O₆ with $\beta = 6.27$ [27], the tetrahedrite Cu₁₂Sb₄S₁₃ with $\beta = 58$ [33], and the type-I clathrate Ba₈Ga₁₆Sn₃₀ with $\beta = 24-25$ [34-36].

Since the magnitude of β is directly related to the coefficient of the 4th order term in the anharmonic potential, the small β of BaIr_2Ge_7 suggests the weakness of the anharmonicity and is in good correspondence with the small ADP parameter[13]. Therefore, our analysis suggests that the temperature dependence of the electrical resistivity and the photoemission spectra can be reproduced and explained in a unified manner by assuming the contribution of the weak anharmonic phonon modes.

The concave-downward behavior of the electrical resistivity has been observed in the various compounds such as the rattling materials and A-15 compounds[26, 37–39]. These behaviors of the electrical resistivity can be explained by the parallel resistor model considering the IR saturation resistivity[26]. On the other hand, the theoretical studies have suggested that the anharmonic phonon mode gives the concave-downward behavior of the resistivity[27, 28]. However, it is difficult to distinguish the contributions from the saturation resistivity and the anharmonic phonon mode. The photoemission spectroscopy can observe the inverse of the QP lifetime directly. In the present study, the temperature dependence of the inverse of the lifetime deduced from the photoemission spectra exhibits the concave-downward behavior, which is in contrast to the temperature-independent lifetime due to the IR scattering. Thus, we have revealed that the spectroscopic analysis can distinguish the contribution between the anharmonic mode and the impurity scattering. This analytical method by using the temperature dependence of the photoemission spectra is a pilot case and can be applied to other systems.

The temperature dependence of the photoemission spectra, the electrical resistivity, and the specific heat suggests the existence of the anharmonic phonon modes. Whether the anharmonic phonon mode originating from the rattling motion works as the glue of the Cooper pair or not is still an open question. Our results indicate that the coupling between electrons and the weak anharmonic phonons mainly contributes to the formation of the quasiparticle. We speculate that the electron-anharmonic phonon coupling may be responsible for the mechanism of superconductivity in BaIr_2Ge_7 .

IV. CONCLUSION

We have investigated the electronic structure of BaIr_2Ge_7 by means of ARPES and HAX-PES measurements. The multi-band FSs with the two-fold symmetry due to the C_2 crystal

structure were observed. From the core-level and valence band photoemission spectra, the near- E_F spectra consist of the strongly hybridized Ir $5d$ and Ge $4p$ orbitals and show the covalent bonding character. The temperature dependence of the valence band spectra reveals the thermal spectral broadening, suggesting the electron-phonon interaction. On the basis of the anharmonic phonon mode, we have reproduced the temperature dependence of the spectral width and the electrical resistivity. The deduced phonon frequencies are consistent with the Einstein temperatures estimated from the specific-heat measurement. Moreover, the anharmonicity factor is relatively small compared with the other rattling materials. Our results suggest that the anharmonic phonon modes exist but the electron-rattler interaction is weak.

ACKNOWLEDGMENTS

The authors would like to thank S. Souma and T. Sato for the technical assistance of BL-28A at Photon Factory and D. Shimonaka, Y. Takasuka, A. Hishikawa, Y. Yuzawa for experimental supports. This work was supported by Japan Society for the Promotion of Science (JSPS) Grants-in-Aid for Scientific Research (KAKENHI Nos. JP16K05445, JP19H05823, JP20H01861, and JP21K13882) and JST SPRING, Grant Number JPMJSP2110. The synchrotron radiation experiments were performed with the approval of SPring-8 (Proposal Nos. 2017A1406 and 2022A1579) and Photon Factory (proposal Nos. 2015G704, 2015S2-003, 2018S2-001, 2019G122, and 2022G077).

-
- [1] L. R. Testardi, *Rev. Mod. Phys.* **47**, 637 (1975).
 - [2] D. Dew-Hughes, *Cryogenics* **15**, 435 (1975).
 - [3] T. Cuk, D. Lu, X. Zhou, Z.-X. Shen, T. Devereaux, and N. Nagaosa, *Phys. Status Solidi (b)* **242**, 11 (2005).
 - [4] A. Chubukov, *Annu. Rev. Condens. Matter Phys.* **3**, 57 (2012).
 - [5] I. Errea, M. Calandra, C. J. Pickard, J. Nelson, R. J. Needs, Y. Li, H. Liu, Y. Zhang, Y. Ma, and F. Mauri, *Phys. Rev. Lett.* **114**, 157004 (2015).
 - [6] V. Keppens, D. Mandrus, B. C. Sales, B. C. Chakoumakos, P. Dai, R. Coldea, M. B. Maple, D. A. Gajewski, E. J. Freeman, and S. Bennington, *Nature* **395**, 876-878 (1998).

- [7] G. S. Nolas, J. L. Cohn, G. A. Slack, and S. B. Schujman, *Appl. Phys. Lett.* **73**, 178 (1998).
- [8] Z. Hiroi, S. Yonezawa, Y. Nagao, and J. Yamaura, *Phys. Rev. B* **76**, 014523 (2007).
- [9] M. Falmbigl, A. Grytsiv, P. Rogl, G. Giester, *Intermetallics*, **36**, 61-72 (2013).
- [10] J. Guo, J. I. Yamaura, H. Lei, S. Matsuishi, Y. Qi, and H. Hosono, *Phys. Rev. B* **88**, 140507(R) (2013).
- [11] M. Falmbigl, F. Kneidinger, M. Chen, A. Grytsiv, H. Michor, E. Royanian, E. Bauer, H. Effenberger, R. Podloucky, and P. Rogl, *Inorg. Chem.* **52**, 931 (2013).
- [12] H. D. Nguyen, Y. Prots, W. Schnelle, B. Böhme, M. Baitinger, S. Paschen, Y. Grin, *Z. Anorg. Allg. Chem.* **640**, 760-767 (2014).
- [13] S. Ishida, Y. Yanagi, K. Oka, K. Kataoka, H. Fujihisa, H. Kito, Y. Yoshida, A. Iyo, I. Hase, Y. Gotoh, and H. Eisaki, *J. Am. Chem. Soc.* **136**, 5245-5248 (2014).
- [14] C. Pei, T. Ying, Y. Zhao, L. Gao, W. Cao, C. Li, H. Hosono, and Y. Qi, *Matter Radiat. Extremes* **7**, 038404 (2022).
- [15] K. Homma and F. Izumi, *J. Appl. Crystallogr.* **44**, 1272 (2011).
- [16] M. Kitamura, S. Souma, A. Honma, D. Wakabayashi, H. Tanaka, A. Toyoshima, K. Amemiya, T. Kawakami, K. Sugawara, K. Nakayama, K. Yoshimatsu, H. Kumigashira, T. Sato, and Koji Horiba, *Review of Scientific Instruments* **93**, 033906 (2022).
- [17] P. Blaha, K. Schwarz, G. K. H. Madsen, D. Kvasnicka, and J. Luitz, *WIEN2k* (Technische Universität Wien, Austria, 2002).
- [18] J. P. Perdew, K. Burke, and M. Ernzerhof, *Phys. Rev. Lett.* **77**, 3865 (1996).
- [19] T. Rachi, M. Kitajima, K. Kobayashi, F. Guo, T. Nakano, Y. Ikemoto, K. Kobayashi, and K. Tanigaki, *J. Chem. Phys.* **123**, 074503 (2005).
- [20] J. Tang, Z. Li, J. Ju, R. Kumashiro, M. A. Avila, K. Suekuni, T. Takabatake, F. Guo, K. Kobayashi, K. Akai, and K. Tanigaki, *Sci. Technol. Adv. Mater.* **9**, 044207 (2008).
- [21] B. A. McDougall, T. Balasubramanian, and E. Jensen, *Phys. Rev. B* **51**, 13891 (1995).
- [22] J. J. Paggel, T. Miller, and T.-C. Chiang, *Phys. Rev. Lett.* **83**, 1415 (1999).
- [23] F. Reinert, B. Eltner, G. Nicolay, D. Ehm, S. Schmidt, and S. Hübner, *Phys. Rev. Lett.* **91**, 186406 (2003).
- [24] Richard C. Hatch, David L. Huber, and Hartmut Höchst, *Phys. Rev. Lett.* **104**, 047601 (2010).
- [25] P. B. Allen and W. W. Schulz, *Phys. Rev. B* **47**, 14434 (1993).

- [26] H. Wiesmann, M. Gurvitch, H. Lutz, A. Ghosh, B. Schwarz, Myron Strongin, P. B. Allen, and J. W. Halley, *Phys. Rev. Lett.* **38**, 782 (1977).
- [27] T. Dahm and K. Ueda, *Phys. Rev. Lett.* **99**, 187003 (2007).
- [28] G. D. Mahan and J. O. Sofo, *Phys. Rev. B* **47**, 8050 (1993).
- [29] F. Bloch, *Z. Phys.* **59**, 208 (1930).
- [30] E. Gruneisen, *Ann. Physik* **408**, 530 (1933).
- [31] T Valla, AV Fedorov, PD Johnson, BO Wells, SL Hulbert, Qiang Li, GD Gu, and N Koshizuka, *Science* **285**, 2110 (1999).
- [32] Y. Nakai, K. Ishida, H. Sugawara, D. Kikuchi, and H. Sato, *Phys. Rev. B* **77**, 041101(R) (2008).
- [33] N. Ghassemi, X. Lu, Y. Tian, E. Conant, Y. Yan, X. Zhou, and J. H. Ross, Jr., *ACS Appl. Mater. Interfaces* **10**, 36010-36017 (2018).
- [34] X. Zheng, S. Y. Rodriguez, and J. H. Ross, Jr., *Phys. Rev. B* **84**, 024303 (2011).
- [35] X. Zheng, S. Y. Rodriguez, L. Saribaev, and J. H. Ross, Jr., *Phys. Rev. B* **85**, 214304 (2012).
- [36] H. Tou, K. Sonoda, K. Furumoto, H. Kotegawa, K. Suekuni, M. A. Avila, and T. Takabatake, *J. Phys. Soc. Jpn.* **82**, 114603 (2013).
- [37] M. Milewits, S. J. Williamson, and H. Taub, *Phys. Rev. B* **13**, 5199 (1976).
- [38] L. R. Testardi, J. M. Poate, and H. J. Levinstein, *Phys. Rev. B* **15**, 2570 (1977).
- [39] R. Caton and R. Viswanathan, *Phys. Rev. B* **25**, 179 (1982).